

4D Printing: Design and Fabrication of Smooth Curved Surface Using Controlled Self-Folding

Dongping Deng, Tsz-Ho Kwok, Yong Chen*

Daniel J. Epstein Department of Industrial and Systems Engineering
University of Southern California
Los Angeles, CA, 90089

*Author of correspondence, Phone: (213) 740-7829, Fax: (213) 740-1120, Email: yongchen@usc.edu

ABSTRACT

Traditional origami structures fold along pre-defined hinges, and the neighboring facets of the hinges are folded to transform planar surfaces into three-dimensional (3D) shapes. In this study, we present a new self-folding design and fabrication approach that has no folding hinges and can build 3D structures with smooth curved surfaces. This four-dimensional (4D) printing method uses a thermal-response control mechanism, where a thermo shrink film is used as the active material and a photocurable material is used as the constraint material on the film. When the structure is heated, the two sides of the film will shrink differently due to the distribution of the constraint material on the film. Consequently, the structure will deform over time to a 3D surface that has no folding hinges. By properly designing the coated constraint patterns, the film can be self-folded into different shapes. The relationship between the constraint patterns and their correspondingly self-folded surfaces has been studied in the paper. Our 4D printing method presents a simple approach to quickly fabricate a 3D shell structure with smooth curved surfaces by fabricating a structure with accordingly designed material distribution.

KEYWORDS: Self-folding; 4D printing; curved surface; smooth folding.

1 Introduction

Self-folding structures have received increased attention in recent years, especially with the demonstration of the four-dimensional (4D) printing concept [1-5]. 4D printing refers to using three-dimensional (3D) printing technology to fabricate structures with heterogeneous materials; upon triggering by external stimuli, the structures can evolve over time (the fourth dimension) to form desired 3D shapes. Self-folding structures have great potential in applications such as micro biomedical devices [6-8], drug delivery systems [9-11], micro reconfigurable robotic systems [12-15], and folded circuit

designs [16-18]. To achieve automatic folding behaviors, different folding mechanisms have been developed, including shape memory polymers (SMPs) [19-21], bilayer structures [22-24], and active hinge-based structures [25-26]. These mechanisms use different materials and designs. Hence the complexity in fabricating them varies significantly; some of them may take a lot of time and effort in preparing and assembling the materials, e.g. the structures with embedded shape memory wires.

Pre-strained polystyrene film has been investigated in self-folding applications due to the easiness of material preparation and low cost. One of the earliest work used black ink and infrared light to achieve self-folding by localizing the absorption of heat on the hinges [27-29]. The film has also been used as an active material in a sandwiched structure by coating or gluing another type of material on it. By carefully designing the parameters on the hinges, well-controlled self-folding could be achieved [30-32]. These self-folding structures are based on origami design, where the shape is composed of flat facets, and the structure folding happens at the hinge portions. However, a lot of product designs, as well as the objects in nature, have shapes with smooth curved surfaces. There is a great need for fabricating curved surfaces, especially for wearable devices whose shapes are required to conform to the surface of a human body.

This paper presents a method to self-fold thin shell structures with smooth curved surfaces using constrained thermal deformation. Since no hinges are used, we name such a self-folding method as "curved folding". The principle of the method is illustrated in Fig. 1. A bilayer structure design is used in the thermal-response control mechanism, where a photocurable resin material (thickness $\sim 0.1\text{mm}$) is coated on the pre-strained polystyrene film (thickness $\sim 0.3\text{mm}$) using the mask-image-projection-based stereolithography (MIP-SL) process, where a mask image is projected onto a thin layer of liquid resin to selectively solidify it. With no constraints, the polystyrene film shrinks almost uniformly in the XY plane under homogeneous heating environment. However, when the resin material is coated on one side of the film, it provides extra physical constraint to the film. Consequently, when the bilayer structure is heated, the resin material has a small shrinking ratio, while the polystyrene film has a large shrinking ratio. Different shrinking ratios in the two sides of the film generate a curved deformation; consequently, the film would be curved up towards the side that has no constraint material. A bi-directional folding can also be achieved by selectively coating the constraint material on both sides of the film. And, most importantly, different constraint patterns will lead to varying folding behaviors, and accordingly, resulting in different 3D shapes.

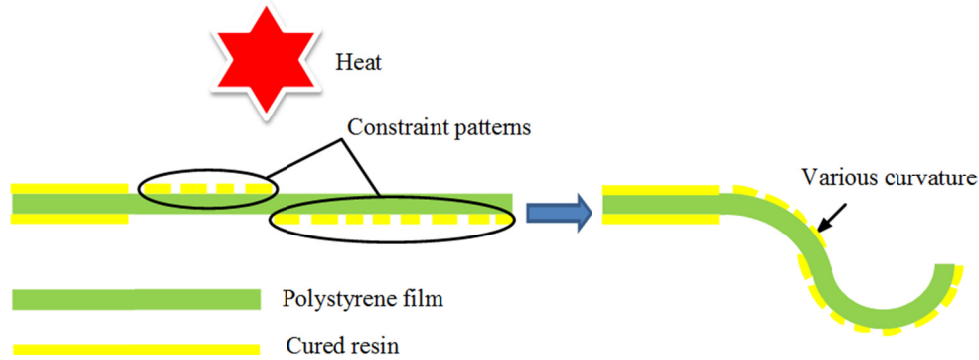


Figure 1. An illustration of the principle of self-folding structures with smooth curved surfaces.

An example of a flower model using the aforementioned curved folding principle is shown in Fig.2. The major challenge is how to design two-dimensional (2D) constraint patterns such that the printed film can have the desired self-folding behavior in order to fabricate a given curved surface. To address the problem, we have developed a design method by mapping a given 3D surface into a set of surface patches, and then generating 2D constraint patterns based on three basic folding features. A number of experiments have been performed to identify proper constraint patterns that can enable the film to achieve the folding behaviors that can be defined by parameters such as the folding axis, curvature, and orientation. A simulation tool has been developed to predict the deformed 3D shape based on an established analytic model. The simulation results have been validated by comparing them with the physical testing results that are captured by a 3D scanner. The rest of the paper is organized as follows. Section 2 introduces a mapping method based on three basic folding types and related folding parameters. Section 3 discusses the effect of different constraint patterns and how to use them to achieve smooth curved surfaces. A developed simulation method is also introduced in the section. Afterwards, Section 4 describes the self-folding design and fabrication method with the experimental results of two test cases. Finally, conclusions are drawn with future work in Section 5.

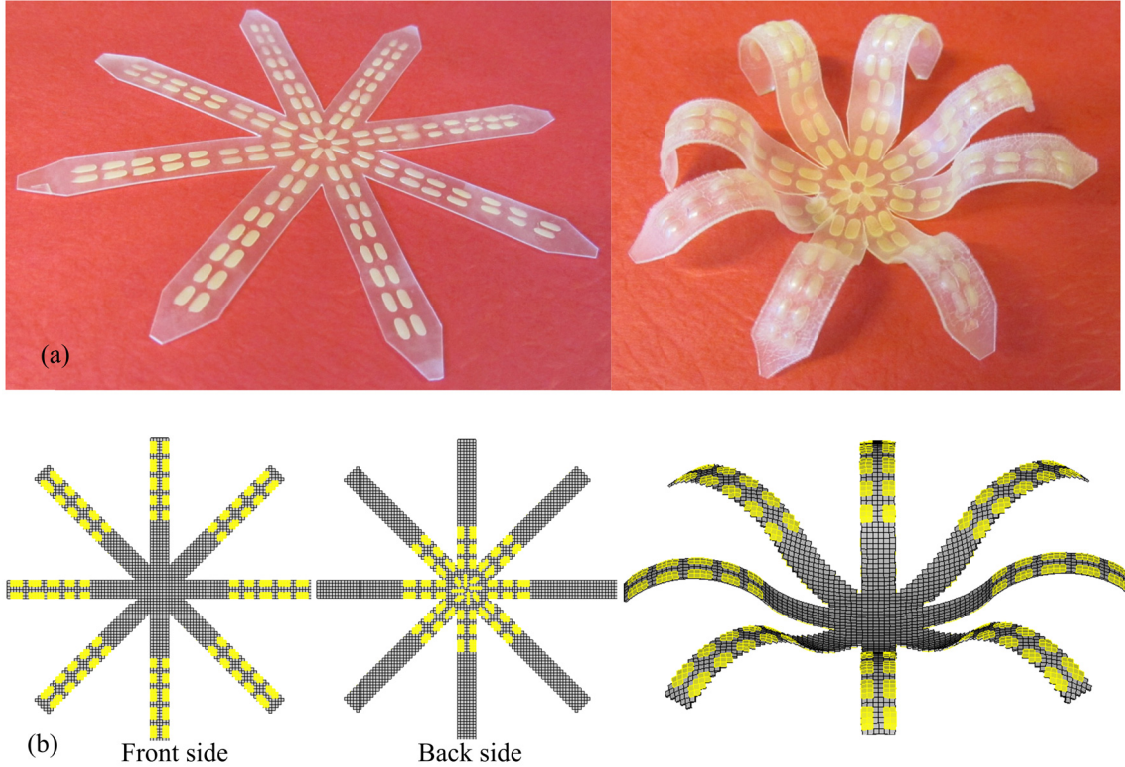


Figure 2. A test case of a self-folding flower. (a) A flower model coated with resin in double-sides and the self-folded object after heating; (b) the simulation results based on a designed constraint pattern.

2 Mapping 3D Thin Shell Structures

2.1 Process Overview

The goal of our study is to develop a self-folding method that can fabricate 3D thin shell structures with smooth curved surfaces. We focus on 3D surfaces that are smooth (i.e., C^1 -continuity over the surface) without sharp features or high curvatures; otherwise, a hinge-based self-folding method (e.g. the one described in our previous work [3, 32]) can be incorporated. Figure 3 shows the main steps of the developed design and fabrication method. For a given 3D thin shell structure, the first step is to unfold the CAD model into a 2D structure with designed constraint patterns through feature mapping. The second step is to fabricate the 2D foldable structure based on the designed constraint patterns. The third step is to fold the fabricated 2D structure into a 3D structure by raising its temperature over the glass transition temperature of the film. Afterwards, an optional step of post-processing can be used, such as coloring, polishing, or assembling multiple 3D structures to form more complex structures.

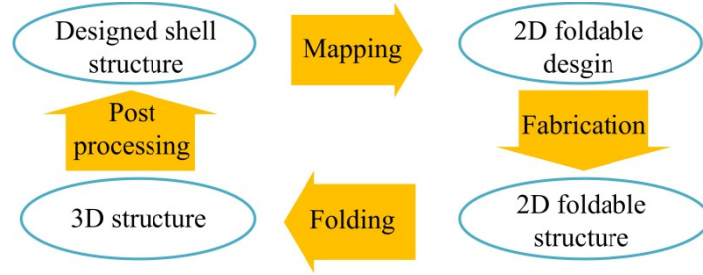


Figure 3. Main steps of the process

2.2 Folding Types and Parameters

A given 3D curved surface can be divided into a set of surface patches based on the idea of shape parameterization and shape matching [33, 34] (refer to Fig. 4a); each of the surface patches is referred as a folding unit in our study. When the surface patch is small, it can be classified into three basic folding types including: (1) flat, i.e., no folding, (2) one-axis, and (3) dual-axis (refer to Fig. 4b). A mapping method is developed for a given curved surface based on this classification. In addition, three folding parameters to define the behavior of a folding unit are folding orientation (flat, upwards, or downwards), folding axis (i.e. the axis along which the surface patch folds), and folding curvature (i.e. how much the flat surface patch curves up). They are shown in Fig.4(c)-4(e), respectively.

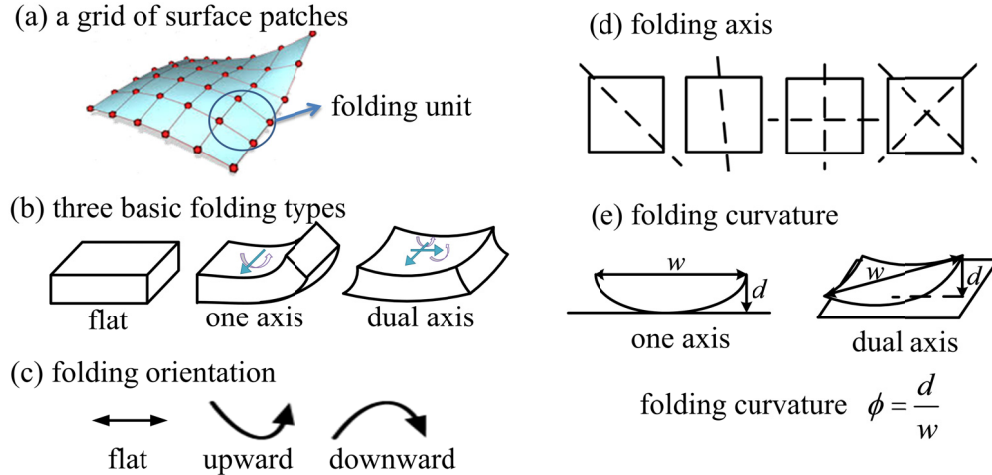


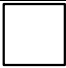


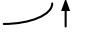
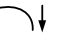
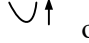
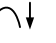
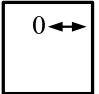
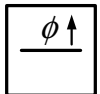

Figure 4. Folding unit and the four folding parameters.

In our study, folding curvature (denoted as ϕ) is defined as the ratio between the depth d (i.e., the height of the flat surface patch curves up) over the width w of the folding unit. The curvature for a flat folding unit is defined as zero. For the type of one-axis folding, the curvature is the depth-to-width ratio of the folded surface patch along the direction that is perpendicular to the folding axis. For the type of dual axis folding, two curvatures (ϕ_1 and ϕ_2) can be defined along the two folding directions respectively.

In this study, we assume the dual-axis folding along the two folding axes is symmetrical. Hence the folding curvature of the surface patch is simplified as the average of ϕ_1 and ϕ_2 .

Accordingly, a set of codes can be defined to label each surface patch based on the aforementioned folding properties. Table 1 shows the codes that are used in the paper to label a surface patch. A square represents the folding unit, and a solid line in the square represents the folding axis. The curvature ϕ is recorded inside the square, and an arrow is used to indicate whether the folding unit folds upwards or downwards. A horizontal double-sided arrow indicates the flat ones.

Table 1. Illustration of folding codes for labeling folding units.

	Flat	One axis	Dual axis
Folding type and axis			
Folding curvature	0	ϕ	ϕ
Folding orientation	\leftrightarrow	 or 	 or 
Examples			

The steps of mapping a 3D structure and generating codes based on the aforementioned classification are shown in Fig. 5. To map a 3D curved surface, the first step is to divide the given surface into a mesh grid based on the idea of mesh parameterization. The patch size can be set by users. Generally, the smaller the size is, the more accurate the mapping would be; however, the required fabrication resolution of the designed constraint pattern will also be higher. The mesh grid defines a set of small surface patches that will be deformed into the 3D curved surface. Based on the defined codes, each surface patch is labeled by its folding type, folding orientation, folding axis, and folding curvature. Fig. 5c and Fig. 5d show the labels of the mesh grids using the codes in Table 1. The constructed surface patches and the accordingly defined folding codes on the patches are the key elements of our self-folding structure design method. We will discuss how to design 2D constraint patterns for each surface patch in Sections 3.

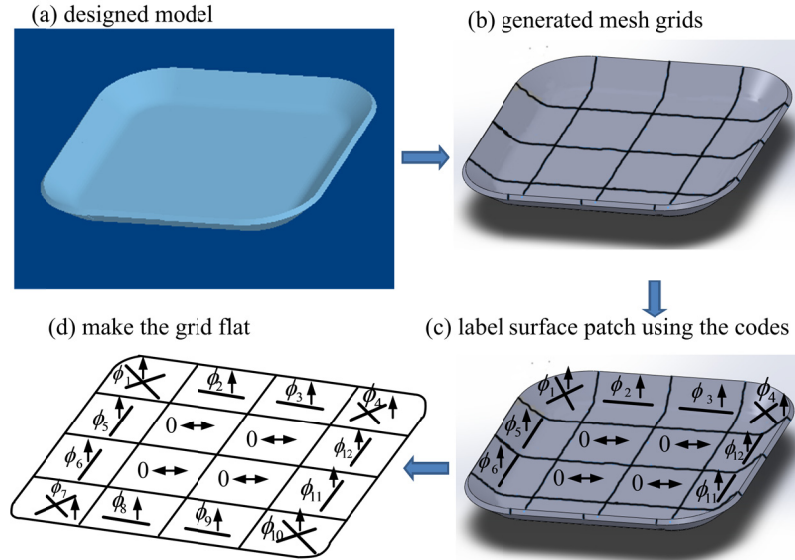


Figure 5. An illustration of mapping a curved surface into a set of folding units.

3 Folding Control Using Constraint Patterns

After a set of coded surface patches have been generated, the design and fabrication of the constraint patterns for them are discussed in this section. The main challenge to be considered is how to convert the folding code of a surface patch to a constraint pattern such that the accordingly fabricated 2D structure, when heated, will be self-folded as designed. As mentioned in Section 1, our method is based on the thermal-responsive control mechanism using a bilayer structure design. That is, a pre-strained polystyrene film serves as the active material, and cured resin is used as the passive material that selectively constrains the shrinkage of the polystyrene film. Both the active and passive materials contribute to the structural deformation. As shown in our previous work [3], heating will cause the film to shrink, which will lead to the deformation of the 2D structure in certain ways. In this section, our study on the shrinkage of a polystyrene film is first presented, followed by a discussion on a correspondingly developed simulation method. Finally, the main factors that contribute to the self-folding behaviors are discussed.

3.1 Shrinkage Study of Polystyrene Film

A polystyrene film is produced by stretching a thick film under heat into a certain thickness and then cooling down rapidly to maintain its stretched shape. Consequently, the film stores a large potential energy (in the form of residual stress) due to the use of stretching to achieve its final shape. When the temperature is raised above its glass transition temperature, the film will release the stored energy and shrink to the most stable configuration. If the pre-stressed polystyrene film is uniformly stretched, it will shrink uniformly on the film plane under heat. However, the stored potential energy of polystyrene film

may not be uniform due to non-uniform processing conditions. Hence the two sides of the film may shrink differently.

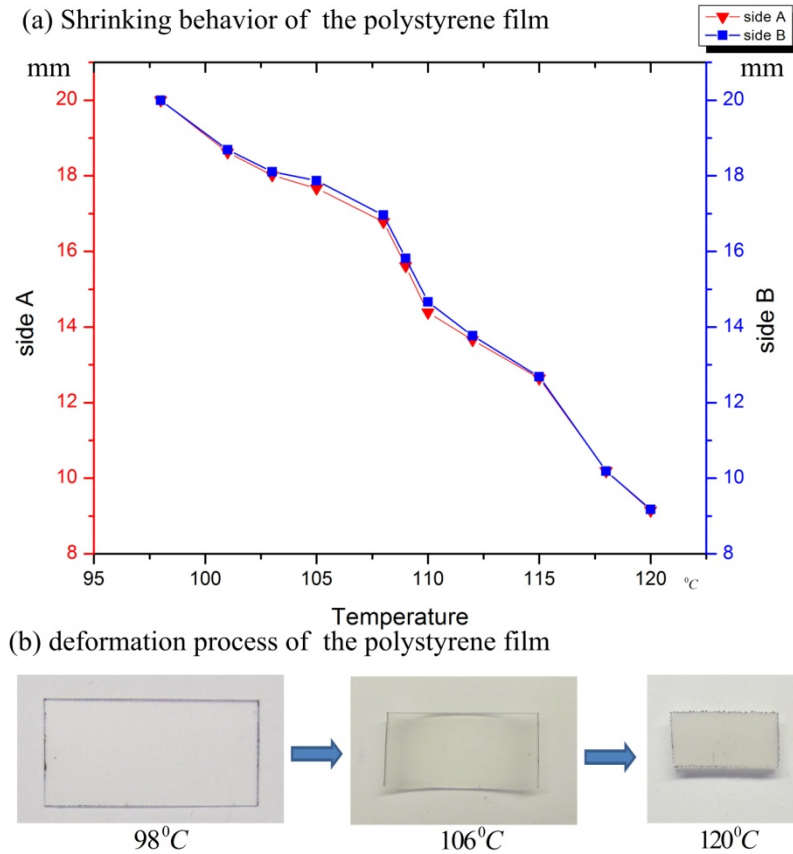


Figure 6. Shrinking behavior of the polystyrene film.

The polystyrene film used in our study is the inkjet shrink film (clear) purchased from Grafix (Maple Hts, OH). Tests were first performed to calibrate its shrinkage ratio by measuring the length of both sides of the film when it is heated to different temperatures. Fig. 6 shows the measured lengths of both sides of the polystyrene film, which has an original length of 20mm. When the temperature is raised up above 98°C, the film starts to shrink, and one side of the film (denoted as Side *A*, red curve) shrinks slightly more than the other side (denoted as Side *B*, blue curve). The difference leads to slight bending of the film at the temperature of 106°C (refer to Fig. 6b). When the temperature keeps increasing, the shrinkage of Side *B* catches up with that of Side *A*; hence the difference becomes smaller. Eventually, the potential energy is totally released when the temperature reaches around 120°C, and both sides shrink similarly to get a flat film in a smaller size (~9mm). For the temperature setting between 98°C and 120°C, each temperature has the corresponding shrinking ratio. The reason is that the polymer chains of the material is not uniform; hence the phase transition is gradually introduced with the increased temperature until the film is totally changed at 120°C. If the temperature keeps on increasing to over 120°C, the film

would become soft or even be melted. Six samples were tested and the same phenomenon is found for all the tested samples with small variation ($<0.2\text{mm}$ or 1% of the original testing length). Hence we used the graph in Fig. 6(a) as the shrinkage estimation of the polystyrene film in our design.

As mentioned before, 2D patterns are designed to constrain one side of the film to achieve the bending of the film towards another side. It is desired to have a small shrinkage difference between the two sides of the film (i.e. Side A and B) such that its effect could be minimized in the pattern design. In addition, if the shrinkage of the film is too large, the shear stress induced between the film and the coated material would be large as well. Consequently, the constraint material may be peeled off from the film. In our study, the shrinkage ratio in all the tests is kept smaller than 25% by using a lower temperature. Based on the curve shown in Fig. 6(a), the raised temperature in our study is set at 108°C , at which the related shrinking difference on the two sides of the film is relatively small.

3.2 Deformation Principle and a Simulation Method

Constraint patterns are designed to cause the polystyrene film to shrink differently on both sides. The shape of the coated constraint material will determine how the fabricated 2D structure will self-fold when heated. The moment of inertia is one of the main parameters to evaluate how a 2D surface patch will bend. As shown in Fig. 7, for a surface patch with thickness h , width b and length a , the moment of inertia

I around the X and Y axes is $I_x = \frac{bh^3}{12}$ and $I_y = \frac{ah^3}{12}$, respectively.

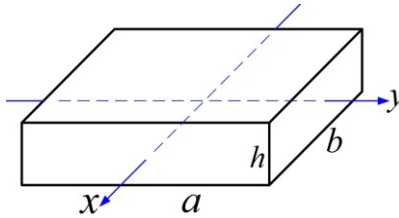


Figure 7. Folding axis analysis.

As the thickness of the constraint layer (h) is fixed, the 2D structure tends to bend around the axis that has a smaller I value. For example, if $b \ll a$, the surface patch will bend around the X axis. In other words, assuming the film portions that are coated with constraint material are protected from heating and constrained by the coated material, the two sides of the film will shrink differently. Hence the distribution of the coated material will lead to the bending of the film around the axis that is orthogonal to the distribution of the constraint material.

A simulation method based on the analyzed deformation principle is developed to predict the deformed 3D shape for a 2D structure with designed constraint patterns. Similar to the finite element method (FEM), we subdivide a design domain into a set of small elements, e.g., small cells as shown in

Fig.8(c). When the elements are sufficiently small, the contraction and deformation can be approximated linearly. In the simulation, we assume the side of a shrinking film without coated material will shrink to a new length $R \cdot L$ that is linearly computed from the original length L as illustrated in Fig. 8(a) with a 2D view.

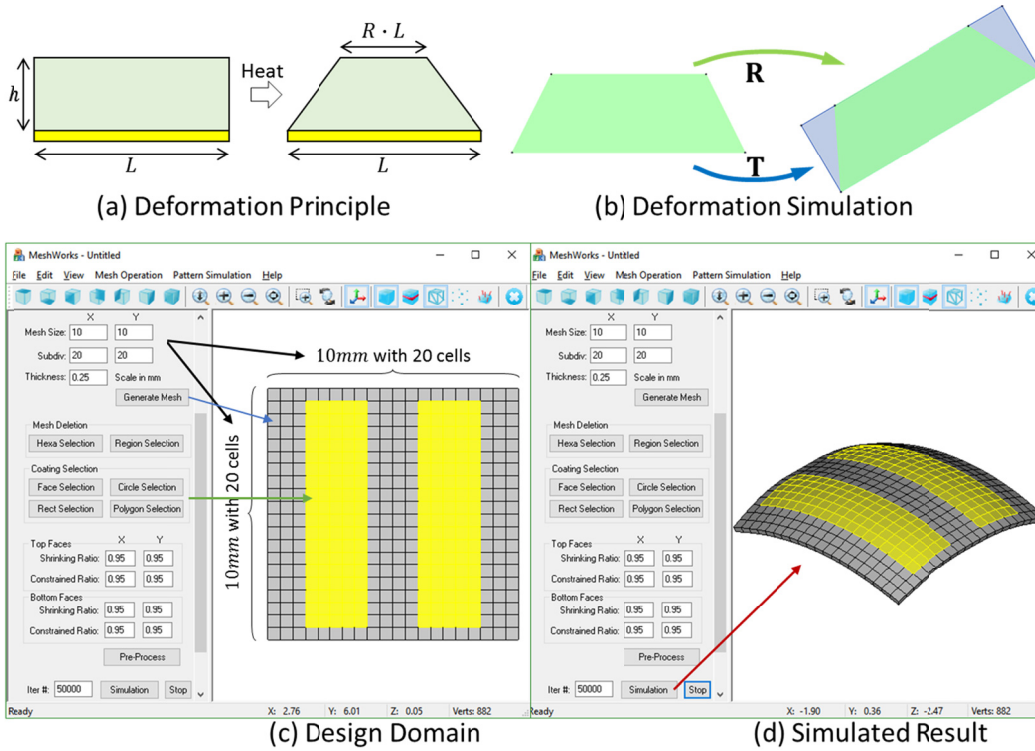


Figure 8. Deformation principle used in simulation and the developed simulation.

Given the shrinkage ratio R , which can be obtained through the calibration tests as shown in Fig.6(a), the target shape of each element can be computed based on the configuration of the constraint patterns. For example, when both sides of the element are constrained, this element will stay the same shape with no deformation throughout the self-folding process. However, when one side of the element is empty and another side is constrained, it is deformed like the one shown in Fig. 8(a). The target shapes can be computed individually for each element; however, when the target shapes of the neighbor elements are putting together, conflicts will arise that need to be resolved by connecting the elements together to approach a target shape with the smallest conflict. Therefore, the simulation is developed by projecting a set of vertices onto the target shape by minimizing the sum of the squared distances of the vertices to the corresponding constraint set. This minimum is computed through shape matching, i.e. by finding the least squares fit of the constraint shape onto the set of vertices. Let V be a vector that stacks all the vertices of the elements (V_1, \dots, V_n) and $V_i \subseteq V$ be the vertices of the i -th element. A new function is developed for the simulation:

$$\mathbf{E} = \sum_{i=1}^m \|\mathbf{N}\mathbf{V}_i - \mathbf{N}\mathbf{V}'_i\|^2 \quad (1)$$

where $\mathbf{N} = \mathbf{I}_{8 \times 8} - \frac{1}{8} \mathbf{1}_{8 \times 8}$ with $\mathbf{1}$ being a matrix with all element equal to 1, and \mathbf{V}'_i is the projected vertices computed by the target shape. Equation (1) can be rewritten to a linear equation system that can be solved by a least square solution:

$$\mathbf{E} = \|\mathbf{A}\mathbf{V} - \mathbf{p}\|^2 \quad (2)$$

where \mathbf{A} is a $8m \times n$ matrix combines all the mean-centered vertices and \mathbf{p} integrates all projections, and the solution of Equation (2) will be the vertex positions of the simulation mesh such as the ones shown in Fig.8(c). In other word, it is trying to maintain the rigidity of the transformation between the target and the current shape of the elements as shown in Fig. 8(b). The computation scheme used in our simulation method is adopted from the ones that have been used in other engineering applications (e.g. [35, 36]). Based on the developed simulation tool, an input 2D structure in Fig.8(c) will lead to a 3D shape with the minimum E as shown in Fig. 8(d). Hence, we can predict the behavior of a designed constraint pattern. We will discuss the constraint pattern design that can be used to achieve the four folding parameters of a folding unit in the following two sections.

3.3 Folding Type and Axis Control Using Constraint Patterns

Since the folding type and the axis direction are highly related, we will discuss them together. As shown in Fig.7, a simple 2D bar ($b \ll a$) can be used as the constraint pattern if a folding axis is defined. The direction of the constraint bar (i.e. the direction of the longest edge) should be perpendicular to the folding axis. Similarly, a 2D cross shape can be used as the constraint pattern for a dual-axis folding. Fig.9 shows the designed constraint patterns with related experimental results for both one-axis and dual-axis folding. Five constraint patterns were tested, and the feasibility of using them to achieve the three basic folding types has been demonstrated. In the designs as shown in Fig.9, the grey portion is the polystyrene film, and the yellow portion is the designed constraint patterns, which are printed using the MIP-SL process [32]. The black lines on the film were drawn in order to position the film during the fabrication process.

As shown in the test results, the folded shapes of both one-axis and dual-axis cases are close to the desired shapes. Simulation results were also computed for the tests. The steps of the comparison analysis are shown in Fig. 10. The folded samples are scanned using a SLS-2 3D Scanner (David Vision Systems GmbH, Germany) with a resolution of 0.06mm. The scan data is then compared with the simulated data. Since a simulated model is based on a 3D object with certain thickness while the related 3D scanned data is a mesh surface, only the exterior surface of the simulated model is used in the

comparison analysis. *Hausdorff* distance is used to evaluate the difference of the two meshes in different data points. The publicly available software system - Metro [37] is used to compute the *Hausdorff* distance between the two meshes. For the test samples with the size of 10mm×10mm, the maximum error is around 0.8mm. It can be noticed that the majority of the comparison color map is in blue color, while the boundaries of the patches have large error, which may be due to the different heating conditions along the boundary.

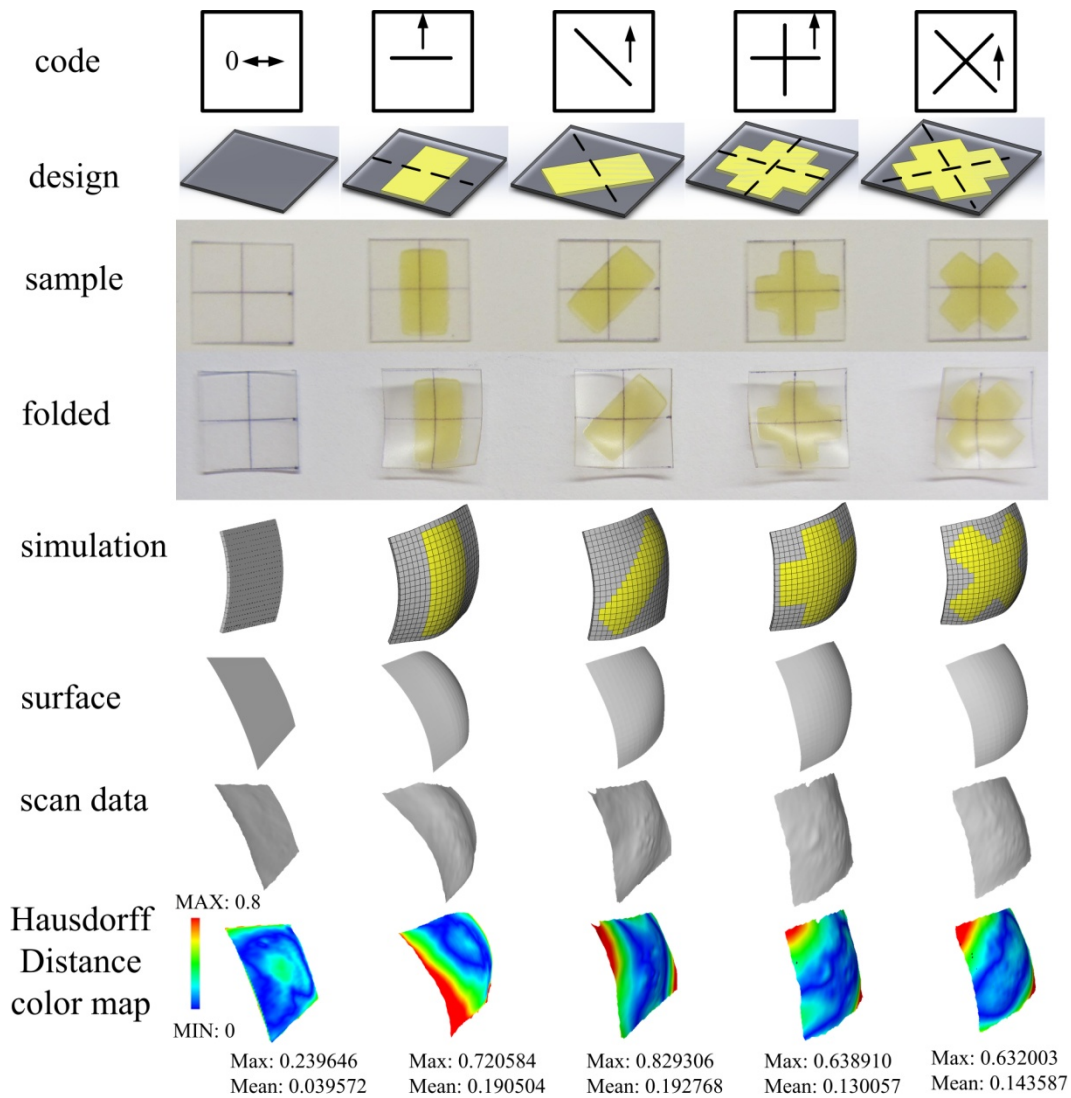


Figure 9. An illustration of the constraint patterns.

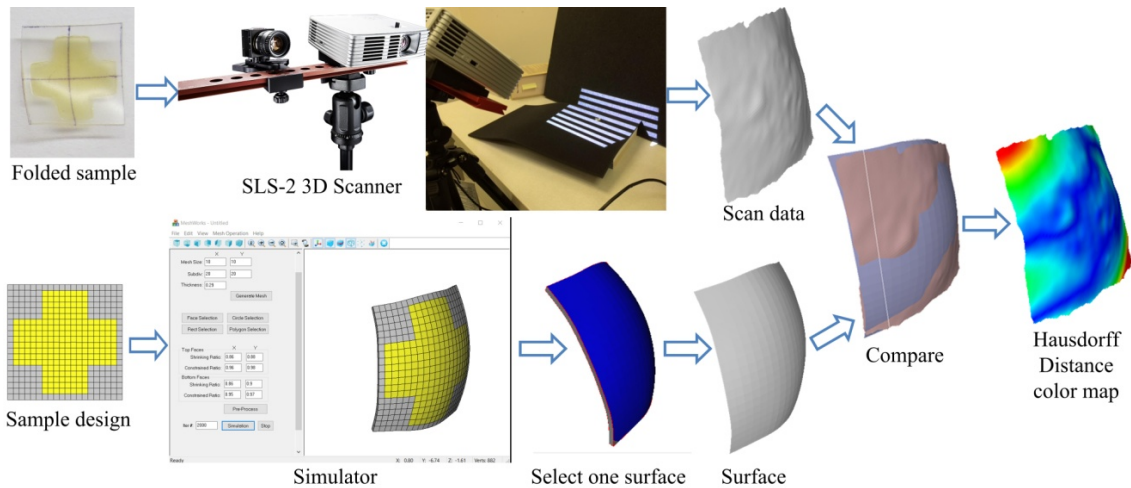


Figure 10. The comparison analysis of a folded model versus a related simulation model.

Some additional experiments were performed to study the folding performance of the one-axis folding type. In the tests, the single constraint bar is subdivided into two and three parallel bars by keeping the total areas of the constraint patterns the same. Fig.11 shows the designed patterns and the folded results. The blue dashed line in the figure indicates the folding axis. After the folding, we evaluated the performance of folding by evaluating the straightness of the curve along the folding axis, which is defined as the axial curve. Theoretically, if the sample is perfectly folded along the axis, the axial curve is a straight line. However, due to the constraint material, the coated portion will curve up and form a "bump". When the constraint pattern is divided into smaller parts, smaller "bumps" will form and the overall smoothness of the structure will be improved. The results show that the more constraint bars used in a 2D structure, the better overall smoothness the structure can obtain. However, the constraint pattern cannot be unlimitedly divided into smaller ones since the fabrication process has a limited feature resolution. In our study, we used three bars as the 2D constraint pattern for the one-axis folding type.

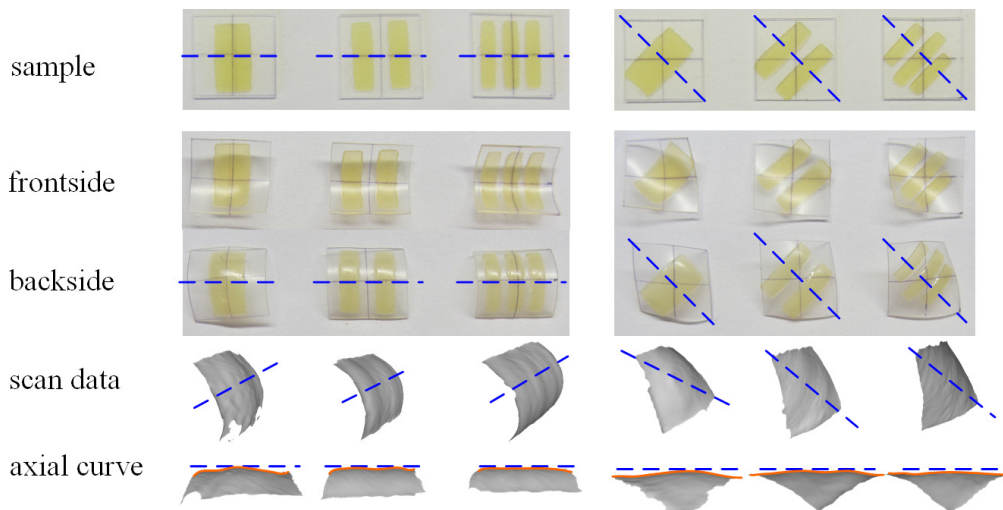


Figure 11. Folding performance of one axis folding using different distributions of materials.

3.4 Folding Curvature and Orientation Control Using Constraint Patterns

Another important parameter to control the folding of a surface patch is the folding curvature. The factors that may affect the curvature of a surface patch include the shape of the constraint pattern, the property of constraint material, the thickness of the constraint layer, and the temperature used in self-folding. In our study we fix all the factors except the shape of the constraint pattern in order to study the relation between the folding curvature and the pattern shape. The effects of other factors will be explored in our future work.

In a folding unit, a constraint pattern for a surface patch can have a wide variety of designs, including its shape, position, and scale. We limited the pattern designs in our study and chose two patterns for the one-axis and dual-axis folding, respectively. As shown in Fig.12, a parallel bar pattern is used for the one-axis folding, and a cross shape pattern is used for the dual-axis folding. Fig.12 also shows the pattern size and position that are considered in our study. The edge length of a unit surface patch is denoted as L . The control parameter in these designs is the width of the constraint bar, that is, l_1 in Fig. 12(a) and l_2 in Fig. 12(b). We experimentally studied how to set the design parameters to achieve the desired folding curvatures.

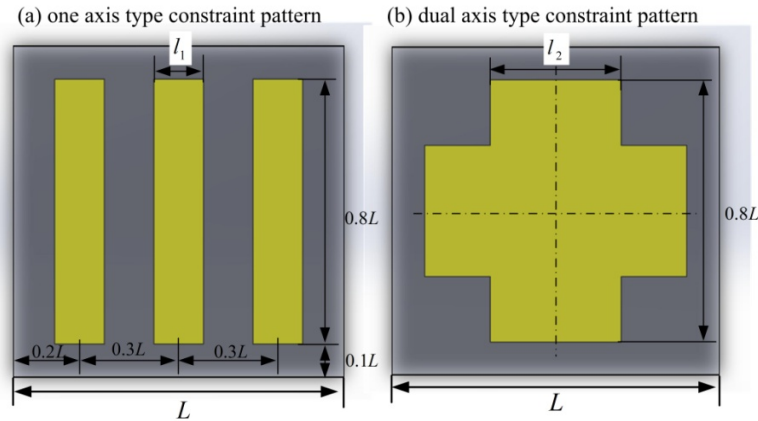


Figure 12. Two constraint pattern examples for two base types.

A set of designed tests were performed to calibrate the relationship between l_1 , l_2 and their corresponding curvatures. The fabricated samples and the folded results are shown in Fig.13 and Fig.14. Similar to Fig. 10, the comparison analysis of the experimented and simulated results were performed. In addition, the values of the depth and width (d, w) as discussed in Section 2.2 were measured using a caliper. Table 2 shows the measurement results. In the tests, the size of each surface patch is 10mm×10mm. Fig.15 shows the plotted curve based on the data in Table 2. The experimental results illustrate that the constraint patterns for both one-axis and dual-axis folding types can be used to control the folding curvatures of the polystyrene film. Increasing the parameter l_1 and l_2 will increase the

curvatures of the corresponding surface patch. In addition, for a polystyrene film without any constraint material (i.e. the cases when l_1 and l_2 equals zero), the curvature is very small compared to the ones with constraint layers. Hence it can be regarded as the flat folding type.

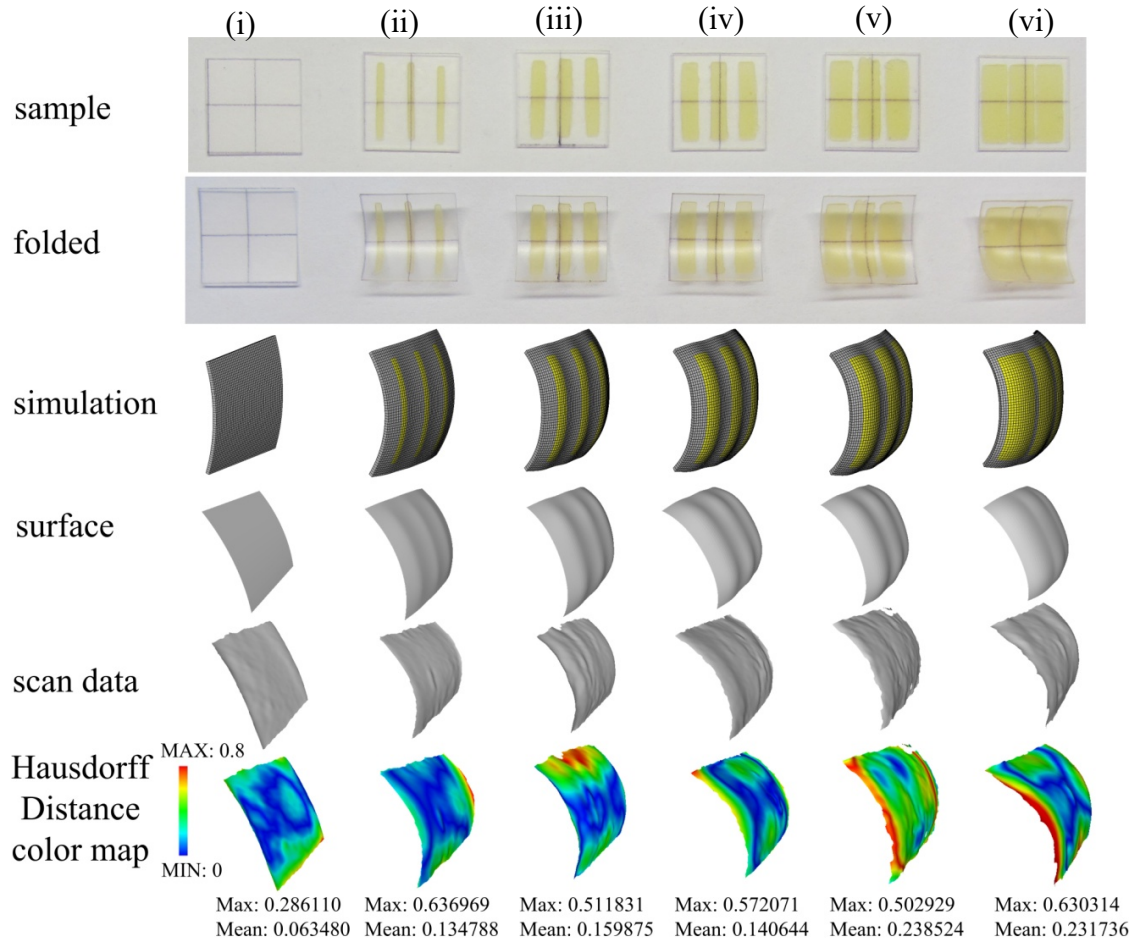


Figure 13. Curvature control with the parallel bar pattern.

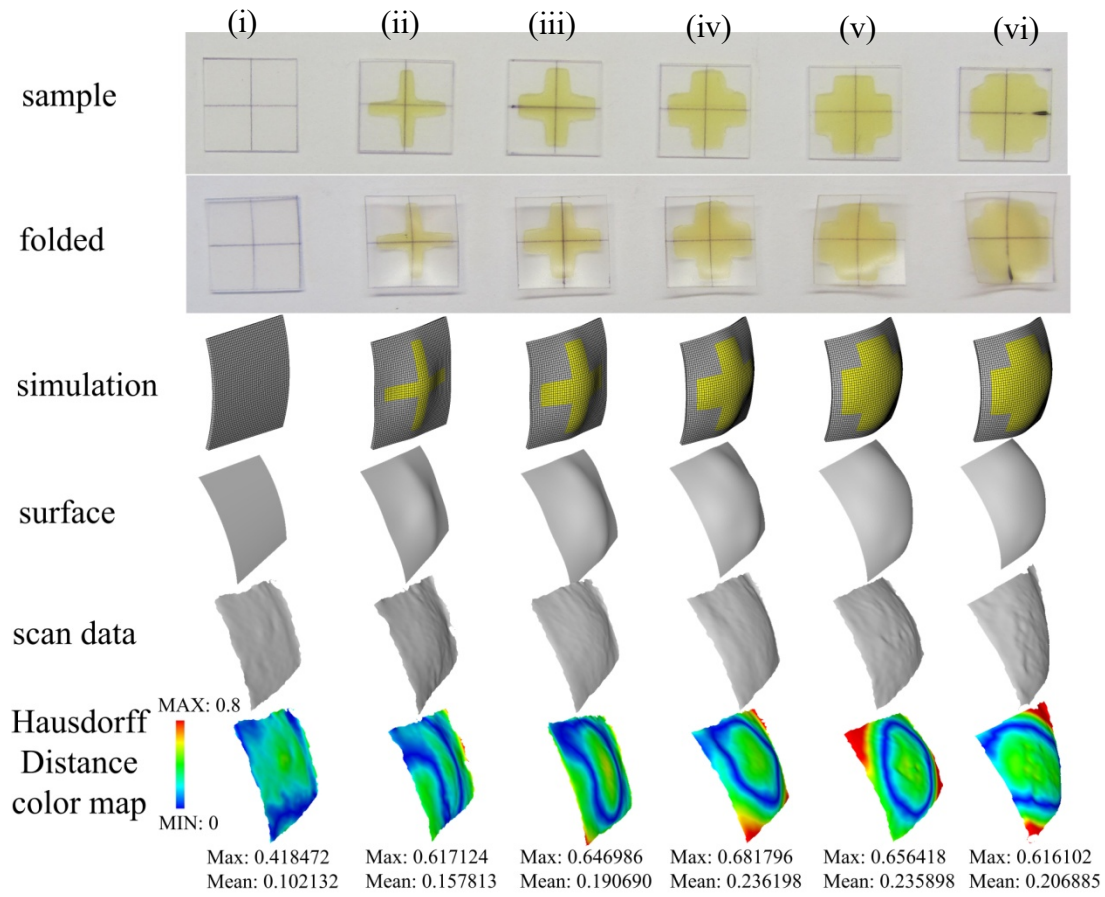


Figure 14. Curvature control with the cross shape pattern.

The relationship between the folding curvature and the parameters of the constraint pattern can be used in designing the required constraint patterns for a given 3D shell structure. For example, for a folded 3D structure with a specific curvature value, we can determine the parameters l_1 (or l_2) by the curves in Fig.15. When there is no exact point for a given value, the parameter is approximated by the linear interpolation between two neighboring data points.

From the measured data, the curvature varies from 0.044 to 0.313. Using our method, it would be difficult to fabricate sharp features that have large curvatures unless the folding units of the related features are further subdivided into smaller surface patches. However, using small surface patches will require a fabrication process that has an even higher resolution. The MIP-SL process used in our study enables the constraint pattern to have feature size as small as 0.5mm.

Finally, the last folding parameter of a folding unit is the folding orientation. The constraint material can be coated on either side of the film. When the constraint pattern is coated on one side of the film, the film will bend towards the other side when heated. Hence, the folding orientation can be easily controlled by coating the resin on the appropriate side of the film.

Table 2. Results of the folding curvature and bar width from Fig.13 and Fig.14.

One Axis Sample	i	ii	iii	iv	v	vi
l_1 (bar width)(mm)	0	0.5	1	1.5	2	2.5
depth d (mm)	0.60	1.99	2.07	2.13	2.35	2.60
width w (mm)	9.63	8.81	8.68	8.69	8.84	8.30
curvature ϕ	0.062	0.226	0.238	0.245	0.266	0.313
Two Axis Sample	i	ii	iii	iv	v	vi
l_2 (bar width)(mm)	0	1	2	3	4	5
depth d (mm)	0.61	1.44	1.53	1.76	2.21	2.46
width w (mm)	13.82	13.23	13.31	13.09	13.03	12.84
curvature ϕ	0.044	0.109	0.115	0.134	0.170	0.192

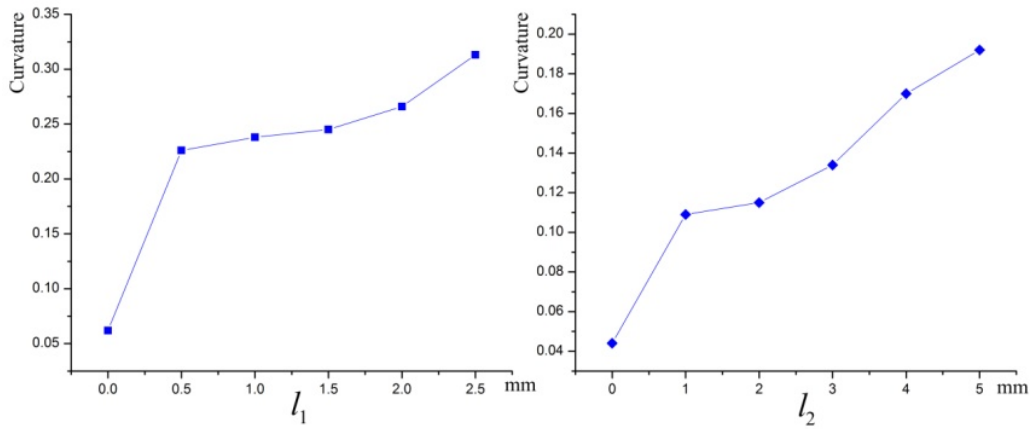


Figure 15. Curvature control curves.

4 Constraint Pattern Design and Fabrication

As discussed in Section 3, a 2D film with varying constraint pattern designs can have different folding performances, which are defined by the four folding parameters on small surface patches. Our 4D printing approach approximates a smooth surface by a set of surface patches with their curvatures. Accordingly, the design process to generate the constraint patterns based on the coded surface patches is shown in

Fig.16. The first step is to calculate the curvatures of each surface patch. A number of points are sampled along the boundary and the center of each surface patch to measure its width and depth in different directions. The direction that has the minimum curvature variation along the sampling direction is selected as the folding axis. If the curvature variation in the orthogonal direction is large (i.e., >0.044 in the test), the additional direction will be selected as the second folding axis, and the dual-axis pattern will be used for the surface patch. To achieve the measured curvature of each surface patch, the curves shown in Fig.15 are used to determine the parameters l_1 and l_2 . Accordingly, the constraint patterns can be designed based on the two patterns developed for the one-axis and dual-axis folding types (refer to Fig.12). Finally, a mask image is generated for coating the constraint material on the polystyrene film, which will be cut into flat 2D shape.

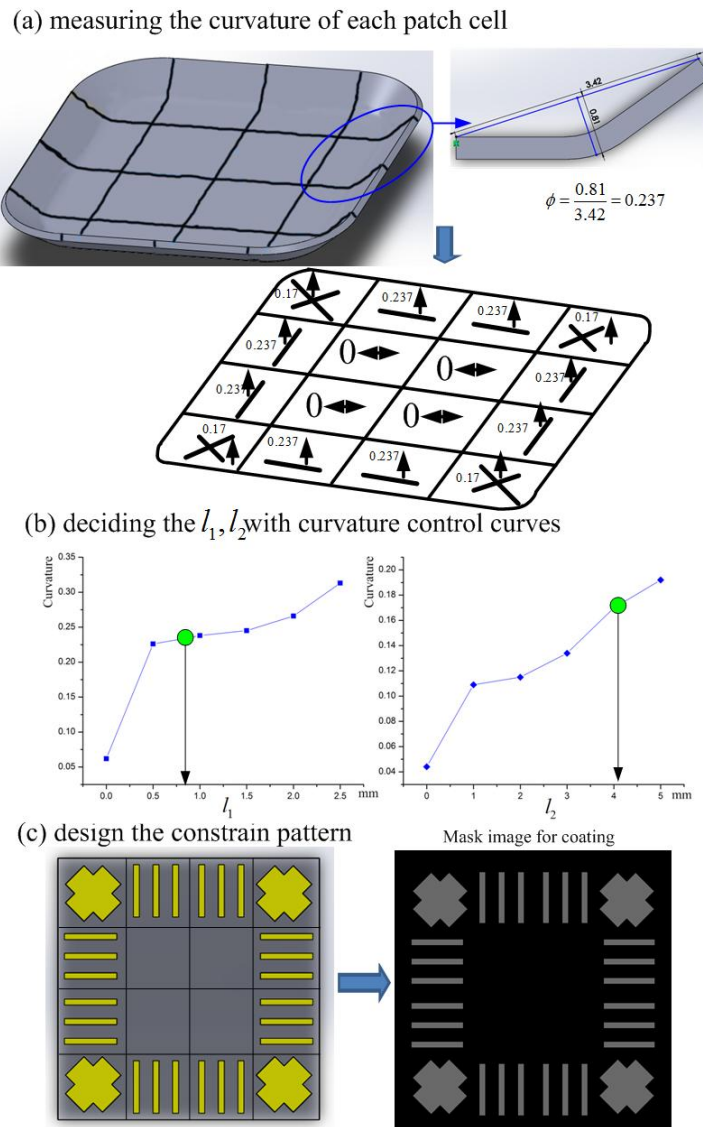


Figure 16. The constraint pattern design process.

Fig.17 shows the fabrication system that was used in our study to print the photocurable resin on the polystyrene film. The fabrication process is based on the MIP-SL process [38-40]. During the fabrication process, a mask image is projected onto the printing chamber. The polystyrene film is positioned on the bottom of the chamber, and a layer of liquid resin is spread on top of the polystyrene film. After that, a transparent cover coated with PDMS film is used to form a thin layer, and the layer thickness is controlled by spacers. When the resin is exposed to the projected image, the photocurable resin gets solidified to form the constraint pattern on the polystyrene film. The resin used in our study is SI500 resin from EnvisionTEC Inc. (Dearborn, MI). The photocuring process will lead to a small temperature increase [41]; however, it will be far lower than the glass transition temperature of the polystyrene film.

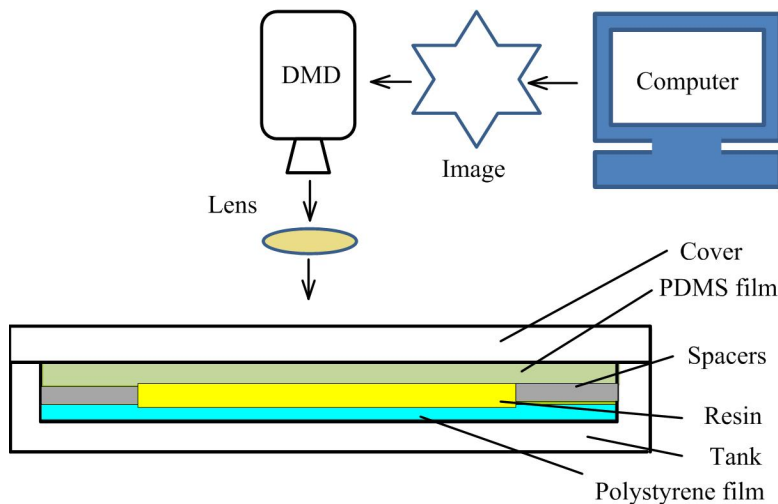


Figure 17. A fabrication system based on the MIP-SL process.

Fig.18 shows the fabricated film with the designed pattern using the MIP-SL process. After positioning the fabricated film inside an oven that is pre-heated to 108°C, the structure is self-folded into the 3D shape as shown in Fig. 18. The self-folded curved surface was captured using the SLS-2 3D scanner and compared with the designed CAD model. The color map of the *Hausdorff* Distance shows that the shapes of the designed and folded models are close to each other. In addition, the folded 3D structure has the desired curve surface that is smooth. The self-folded curved surface has no folding hinges, or stair-stepping effect that is typical in the layer-based AM processes. The fabricated 3D structure can be used as a tool to transfer the shape of the curved surface into other materials such as silicone rubber. In addition, the folding process takes less than 10 seconds, which is much shorter than the fabrication time that is required for building the 3D structure using a 3D printer such as a MIP-SL or fused deposition modeling (FDM) machine.

An additional test case based on “USC” letters is shown in Fig.19. The one-axis folding pattern design is used in the test. Compared with the layer-based 3D printing of these 3D structures, our method

does not require the use of additional support structures. The fabrication time is also largely reduced. Based on the experimental results, the feasibility of using the developed design and fabrication method to build 3D thin-shell structures with smooth curved surfaces has been demonstrated.

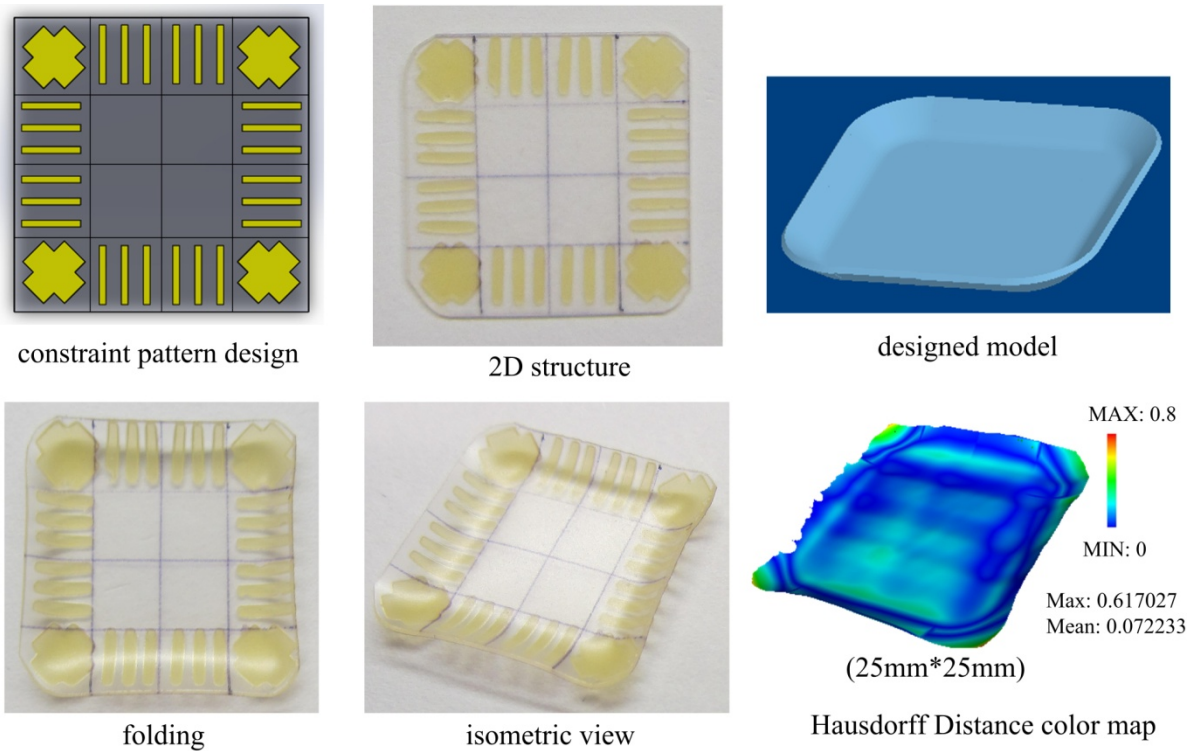


Figure 18. A test case of a bowl.

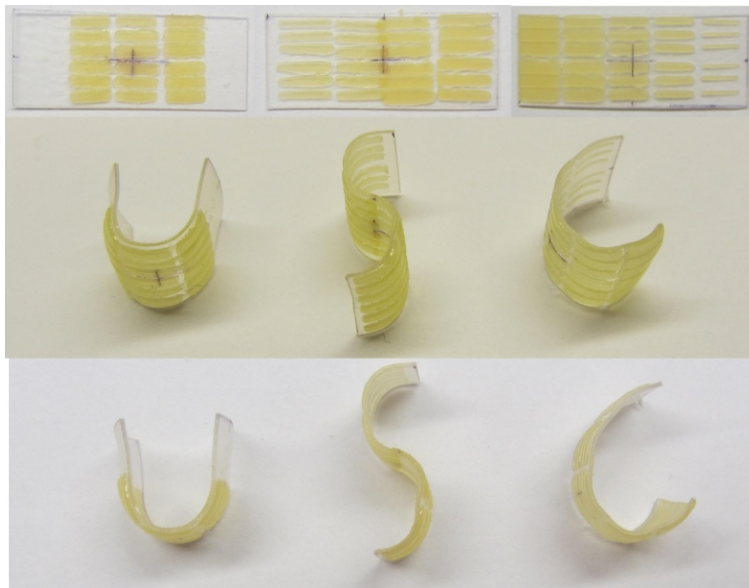


Figure 19. A test case of "USC" letters.

5 Conclusion and Discussion

In the paper a new 4D printing approach to fabricate 3D thin shell structures with smooth curved surfaces has been presented. To control the self-folding process based on a thermal-responsive control mechanism, a curved surface is divided into a set of small surface patches as individual folding units. Each folding unit is classified into three basic folding types: the flat patches, the one-axis folding patches, and the dual-axis folding patches. Three additional parameters are then presented, including folding axis, curvature, and orientation. The effects of these four parameters and the accordingly developed control methods have been presented. In addition, a simulation tool has been developed to predict the deformation of a given constraint pattern. The comparison between the simulated and fabricated shapes shows good agreement. Several test cases have been presented to demonstrate the effectiveness of the developed 4D printing method.

There are several limitations in the presented design and fabrication method. Firstly, the degree of bending is determined by the shrinkage of the polystyrene film. Due to the limit of the shrinkage ratio, our method cannot be used to fabricate shapes with high curvature. Secondly, the thickness of the constraint layer needs to be well controlled. A proper thickness of the constraint layer based on the selected polystyrene film is between 0.1-0.2mm. A concept of digital material by using pixelized constraint materials on the polystyrene film [38, 39] may enable the method to achieve a larger folding curvature range and a wider layer thickness. That is, by using different composition of rigid and soft materials, the printed constraint patterns may have certain flexibility to enable the polystyrene film to have a larger folding curvature range. Finally, the approach that is used to map the 3D shape into 2D surface is based on an approximation of the divided surface patches.

Our future work includes: (1) studying more general constraint 2D patterns and their related control parameters; (2) investigating the use of digital material as the constraint material for self-folding structures; (3) integrating the developed design method with other 4D printing approaches to fabricate more complex structures; and (4) investigating applications that may benefit from the developed process.

REFERENCES

- [1] Tibbits S, 2014, "4D Printing: Multi-Material Shape Change", *Architectural Design*. 84(1):116-21. doi:10.1002/ad.1710
- [2] Ge Q, Dunn CK, Qi HJ, Dunn ML, 2014, "Active origami by 4D printing", *Smart Materials and Structures*. 23(9):1-15. doi:10.1088/0964-1726/23/9/094007
- [3] Kwok TH, Wang CCL, Deng D, Zhang Y, Chen Y, 2015, "4D Printing for Freeform Surfaces: Design Optimization of Origami Structures", *Journal of Mechanical Design*. doi:10.1115/1.4031023

- [4] Bakarich SE, Gorkin R, Panhuis Mih, Spinks GM, 2015, “4D Printing with Mechanically Robust, Thermally Actuating Hydrogels”, *Macromolecular Rapid Communications*; 36(12) :1211-1217. doi:10.1002/marc.201500079
- [5] Mao Y, Yu K, Isakov MS, Wu J, Dunn ML, and Qi HJ, 2015, “Sequential Self-Folding Structures by 3D Printed Digital Shape Memory Polymers”, *Sci. Rep.* 5, 13616; doi: 10.1038/srep13616.
- [6] Randall CL, Kalinin YV, Jamal M, Shah A, Gracias DH, 2011, “Self-folding immunoprotective cell encapsulation devices”, *Nanomedicine: Nanotechnology, Biology, and Medicine*; 7(6): 686-689. doi:10.1016/j.nano.2011.08.020
- [7] Malachowski K, Jamal M, Jin Q, Polat B, Morris CJ, Gracias DH, 2014, “Self-Folding Single Cell Grippers”, *Nano Letters*. 14(7):4164-4170. doi:10.1021/nl500136a
- [8] Breger JC, Yoon C, Xiao R, Kwag HR, Wang MO, Fisher JP, et al, 2015, “Self-folding thermo-magnetically responsive soft microgrippers”, *ACS applied materials & interfaces*. 7(5):3398-3405. doi:10.1021/am508621s
- [9] Guan J, He H, Lee LJ, Hansford DJ, 2007, “Fabrication of particulate reservoir-containing, capsulelike, and self-folding polymer microstructures for drug delivery”, *Small*. 3(3):412-418. doi:10.1002/sml.200600240
- [10] Fernandes R, Gracias DH, 2012, “Self-folding polymeric containers for encapsulation and delivery of drugs”, *Advanced Drug Delivery Reviews*. 64(14):1579-1589. doi:10.1016/j.addr.2012.02.012
- [11] He H., Guan J., Lee JL, 2006, “An oral delivery device based on self-folding hydrogels”, *Journal of Controlled Release*, 110(2), 339-346. doi:10.1016/j.jconrel.2005.10.017
- [12] An B, Benbernou N, Demaine ED, Rus D, 2011, “Planning to fold multiple objects from a single self-folding sheet”, *Robotica*. 29(1):87-102. doi:10.1017/S0263574710000731
- [13] Felton S, Tolley M, Demaine E, Rus D, Wood R, 2014, “Applied origami. A method for building self-folding machines”, *Science (New York, N.Y.)*. 345(6197):644.
- [14] Sun, X., Felton, S. M., Niiyama, R., Wood, R. J., Kim, S, 2015, “Self-folding and self-actuating robots: A pneumatic approach”, Paper presented at the 2015 IEEE International Conference on Robotics and Automation (ICRA), 3160-3165. doi:10.1109/ICRA.2015.7139634.
- [15] Miyashita S, Guitron S, Ludersdorfer M, Sung CR, Rus D, 2015, “An untethered miniature origami robot that self-folds, walks, swims, and degrades”, Paper presented at the 2015 IEEE International Conference on Robotics and Automation (ICRA),1490-1496. doi:10.1109/ICRA.2015.7139386.
- [16] Miyashita S, Meeker L, Tolley MT, Wood RJ, Rus D, 2014, “Self-folding miniature elastic electric devices”, *Smart Materials and Structures*. 23(9):1-9. doi:10.1088/0964-1726/23/9/094005
- [17] Miyashita S, Meeker L, Gouldi M, Kawahara Y, Rus D, 2014, “Self-folding printable elastic electric devices: Resistor, capacitor, and inductor”, Paper presented at the 2014 IEEE International Conference on Robotics and Automation (ICRA), 1446-1453. doi:10.1109/ICRA.2014.6907042.
- [18] Hayes GJ, Liu Y, Genzer J, Lazzi G, Dickey MD, 2014, “Self-Folding Origami Microstrip Antennas”, *IEEE Transactions on Antennas and Propagation*. 62(10):5416-5419. doi:10.1109/TAP.2014.2346188

- [19] Peraza-Hernandez E, Hartl D, Galvan E, Malak R, 2013, “Design and Optimization of a Shape Memory Alloy-Based Self-Folding Sheet”, *Journal of Mechanical Design*. 135(11). doi:10.1115/1.4025382
- [20] Peraza-Hernandez EA, Hartl DJ, Malak Jr RJ, 2013, “Design and numerical analysis of an SMA mesh-based self-folding sheet”, *Smart Materials and Structures*. 22(9):094008,1-17. doi:10.1088/0964-1726/22/9/094008
- [21] Felton SM, Becker KP, Aukes DM, Wood RJ, 2015, “Self-folding with shape memory composites at the millimeter scale”, *Journal of Micromechanics and Microengineering*. 25(8). doi:10.1088/0960-1317/25/8/085004
- [22] Ding Z, Wei P., Ziaie B, 2010, “Self-folding smart 3D microstructures using a hydrogel-parylene bilayer”, the 18th Biennial University/Government/Industry Micro/Nano Symposium ,doi:10.1109/UGIM.2010.5508914.
- [23] Guan J, He H, Hansford DJ, Lee LJ, 2005, “Self-folding of three-dimensional hydrogel microstructures”, *Journal of Physical Chemistry B* 109 (49): 23134-7. doi:10.1021/jp054341g
- [24] De Leon A, Barnes AC, Thomas P, O'Donnell J, Zorman CA, Advincula RC, 2014, “Transfer printing of self-folding polymer-metal bilayer particles”, *ACS Applied Materials & Interfaces* 6 (24): 22695-700. doi:10.1021/am5068172
- [25] Pickett GT, 2007, “Self-folding origami membranes”, *EPL (Europhysics Letters)*. 78(4):48003. doi:10.1209/0295-5075/78/48003
- [26] Guo W, Li M, Zhou J, 2013, “Modeling programmable deformation of self-folding all-polymer structures with temperature-sensitive hydrogels”, *Smart Materials and Structures*. 22(11):115028,1-6. doi:10.1088/0964-1726/22/11/115028
- [27] Liu Y, Boyles JK, Genzer J, Dickey MD, 2012, “Self-folding of polymer sheets using local light absorption”. *Soft Matter*, 8(6), 1764-1769. doi:10.1039/c1sm06564e
- [28] Liu Y, Miskewicz M, Ecsuti MJ, Genzer J, Dickey MD, 2014, “Three-dimensional folding of pre-strained polymer sheets via absorption of laser light”, *J. Appl. Phys.*, 115, 204911. doi:10.1063/1.4880160
- [29] Lee Y, Lee H, Hwang T, Lee J, Cho M, 2015, “Sequential Folding using Light-activated Polystyrene Sheet”, *Sci. Rep.* 5, 16544; doi: 10.1038/srep16544.
- [30] Felton SM, Tolley MT, Shin B, Onal CD, Demaine ED, Rus D, Wood RJ, 2013, “Self-folding with shape memory composites”, *Soft Matter*. 9(32):7688-94. doi:10.1039/c3sm51003d
- [31] Tolley MT, Felton SM, Miyashita S, Aukes D, Rus D, Wood RJ, 2014, “Self-folding origami: shape memory composites activated by uniform heating”, *Smart Materials and Structures*. 23(9):1-9. doi:10.1088/0964-1726/23/9/094006
- [32] Deng D, Chen Y, 2015, “Origami-Based Self-Folding Structure Design and Fabrication Using Projection Based Stereolithography”, *Journal of Mechanical Design (Transactions of the ASME)*. 137(2). doi:10.1115/1.4029066

- [33] Yonekura, K., & Watanabe, O. 2014, "A shape parameterization method using principal component analysis in applications to parametric shape optimization". *Journal of Mechanical Design*, 136(12), 121401. doi:10.1115/1.4028273
- [34] Murray, A., J. Schmiedeler, and B. Korte, 2008, "Kinematic synthesis of planar, shape-changing rigid-body mechanisms". *ASME Journal of Mechanical Design*, DOI: 10.1115/1.2829892
- [35] Bouaziz S, Deuss M, Schwartzburg Y, Weise T, Pauly M. 2012. "Shape-up: shaping discrete geometry with projections". *Computer Graphics Forum*. 31(5): 1657-1667. doi: 10.1111/j.1467-8659.2012.03171
- [36] Xie W, Zhang Y, Wang C, Chung R. 2014. "Surface-from-gradients: an approach based on discrete geometry processing," *IEEE Conference on Computer Vision and Pattern Recognition*, Columbus, OH, 2014, pp. 2203-2210. doi: 10.1109/CVPR.2014.282
- [37] Cignoni P, Rocchini C, Scopigno R. 1998. "Metro: Measuring error on simplified surfaces". *Computer Graphics Forum*, 17: 167–174. doi:10.1111/1467-8659.00236
- [38] Huang P, Deng D, Chen Y, 2013, "Modeling and fabrication of heterogeneous three-dimensional objects based on additive manufacturing", 24th International SFF Symposium - An Additive Manufacturing Conference, SFF 2013. 2013:215-230
- [39] Zhou C, Chen Y, Yang Z, Khoshnevis B, 2013, "Digital material fabrication using mask-image-projection-based stereolithography", *Rapid Prototyping Journal*. 19(3):153-65. doi:10.1108/13552541311312148
- [40] Song X, Chen Y, Lee TW, Wu S, Cheng L, 2015, "Ceramic fabrication using Mask-Image-Projection-based Stereolithography integrated with tape-casting", *Journal of Manufacturing Processes*. 20:456-64. doi:10.1016/j.jmapro.2015.06.022
- [41] Xu K, Chen, Y. 2016, "Photocuring temperature study for curl distortion control in projection based Stereolithography". *Journal of Manufacturing Science and Engineering*. 139(2): 021002. doi: 10.1115/1.4034305.